Free Radical Biology and Medicine 224 (2024) 707–722

Contents lists available at ScienceDirect

Free Radical Biology and Medicine

journal homepage: www.elsevier.com/locate/freeradbiomed

Platycodin D ameliorates polycystic ovary syndrome-induced ovarian damage by upregulating CD44 to attenuate ferroptosis

Rui Ji [a,b], Shujun Wang [c], Xin Chen [a,b], Zhe Yang [a,b], Zhimo Zhang [a,b], Shenglan Bao [a,b], Zhuoni Xiao [a,b,**], Yan Zhang [d,***], Tailang Yin [a,b,****], Jing Yang [a,b,*]

[a] Reproductive Medical Center, Renmin Hospital of Wuhan University, Wuhan, China
[b] Hubei Clinic Research Center for Assisted Reproductive Technology and Embryonic Development, Wuhan, China
[c] Department of Obstetrics and Gynecology, Renmin Hospital of Wuhan University, Wuhan, China
[d] Department of Clinical Laboratory, Renmin Hospital of Wuhan University, WuHan, China

ARTICLE INFO

Keywords:
Polycystic ovary syndrome (PCOS)
Ferroptosis
Platycodin D
CD44

ABSTRACT

Recently, the potential association between polycystic ovary syndrome (PCOS) development and progression and ferroptosis has garnered attention. Increasing evidence suggests that targeting ferroptosis may be an effective strategy for treating PCOS. First, we observed that the expression of the ferroptosis regulatory molecules SLC7A11, GPX4, and FTH1 was decreased in the granulosa cells (GCs) of patients with PCOS and ovarian tissues of rats with PCOS; in contrast, TFR1 expression was increased. This suggests that GC ferroptosis is involved in PCOS pathogenesis. Furthermore, bioinformatics analysis of GC datasets from patients with PCOS and PCOS clinical samples and animal model analysis revealed CD44 as a key molecule regulating ferroptosis in PCOS, which was down-regulated in GCs of PCOS patients and rats. Subsequently, molecular docking was performed to screen existing natural compounds for inhibiting ferroptosis. Dynamic simulation and cellular thermal shift assay identified platycodin D as a natural plant extract for inhibiting ferroptosis by targeting CD44 in GCs. Subsequently, a series of functional experiments revealed that platycodin D ameliorated ovarian damage in rats with PCOS. This was primarily owing to the protective effects achieved by promoting glutathione production, attenuating lipid accumulation and lipid peroxidation in GCs, inhibiting iron overload, and scavenging reactive oxygen species. In addition, western blotting and immunofluorescence staining revealed that platycodin D upregulated the expression of CD44 and SLC7A11 in GCs. Furthermore, by knocking down CD44 and SLC7A11 *in vivo* and *in vitro*, respectively, the ameliorative effect of platycodin D on ferroptosis in the GCs of rats with PCOS was reversed. Collectively, these findings suggest that platycodin D attenuates ferroptosis in GCs by activating CD44/SLC7A11 axis, thereby upregulating system X_c^-. In conclusion, platycodin D can attenuate ferroptosis in GCs by activating CD44, potentially ameliorating ovarian damage in PCOS.

1. Introduction

Polycystic ovary syndrome (PCOS) is a common reproductive endocrine disease that occurs in women of fertile age. It is primarily characterized by sporadic ovulation and polycystic ovarian changes, generally accompanied by clinical characteristics such as hyperandrogenemia, glucose and lipid metabolism anomalies, and chronic low-grade inflammation [1]. Recently, the diagnosis rate of PCOS has been gradually increasing, affecting women's reproductive health and imposing heavy physical and mental burdens on women of childbearing age [2]. At present, metabolic abnormalities and menstrual disorders in patients with PCOS are primarily addressed through lifestyle modifications, including the use of metformin and weight loss, as well as the incorporation of combination contraceptives and surgical procedures. However, the improvement in patients' quality of life and fertility outcomes remains limited. Furthermore, the use of hormone drugs and

* Corresponding authors. Reproductive Medical Center, Renmin Hospital of Wuhan University, Wuhan, China.
** Corresponding author. Reproductive Medical Center, Renmin Hospital of Wuhan University, Wuhan, China.
*** Corresponding authors.
**** Corresponding author. Reproductive Medical Center, Renmin Hospital of Wuhan University, Wuhan, China.
E-mail addresses: RM001111@whu.edu.cn (Z. Xiao), peneyyan@whu.edu.cn (Y. Zhang), reproductive@whu.edu.cn (T. Yin), dryangjing@whu.edu.cn (J. Yang).

https://doi.org/10.1016/j.freeradbiomed.2024.09.033
Received 15 July 2024; Received in revised form 10 September 2024; Accepted 22 September 2024
Available online 24 September 2024

surgical procedures may increase the risk of thromboembolism and infection [3]. Previous studies have revealed that programmed cell death contributes to PCOS pathophysiology by damaging ovarian granulosa cells (GCs). Recent studies have suggested that ferroptosis owing to hyperandrogenemia contributes to PCOS progression [4].

Ferroptosis is a type of regulated iron-dependent cell death. It is characterized by the accumulation of redox-active iron (ROS), dysregulation of resistance to oxidative stress, and impairment of lipid peroxide metabolism [5]. Evidence suggests an association between ferroptosis and the development of diabetes mellitus, cardiovascular diseases, tumors, and neurodegenerative diseases [6]. Therefore, regulating ferroptosis occurrence may be a beneficial approach for treating various diseases. Recently, the regulation of ferroptosis in female reproductive system diseases has garnered attention [7]. Furthermore, recent studies have revealed the association between dysregulation of ferroptosis-regulating genes in GCs and impaired oocyte quality in patients with PCOS [8]. Furthermore, in animal experiments, researchers noted that hyperandrogenemia and insulin resistance activated ferroptosis in the uterus and placenta of pregnant rats; this resulted in the occurrence of fetal miscarriages [9]. In addition, miR-93-5p levels were increased in ovarian GCs of patients with PCOS, resulting in the ferroptosis of GCs via the nuclear factor kappa B signaling pathway. The inhibition of miR-93-5p effectively improved GC dysfunction [10]. Another study has revealed that metformin can attenuate the ferroptosis of GCs via the SIRT3/AMPK/mTOR pathway, thereby improving metabolic disorders and ovarian dysfunction in mice with PCOS [11]. Therefore, ferroptosis may play an essential regulatory role in PCOS pathophysiology. Exploring the targeted regulation of ferroptosis may help alleviate the current challenges in PCOS treatment.

CD44 is a transmembrane glycoprotein with multiple structures and functions on the cell surface. It is a member of the cartilaginous connectin protein family [12]. CD44 is commonly expressed in epithelial cells, including lymphocytes, fibroblasts, and smooth muscle cells. Its vital role in the physiological processes of both normal and cancer cells has been comprehensively investigated. Studies have revealed that CD44 participates in various biological activities, including cell proliferation, cell differentiation, cell migration, and membrane docking of proteases and signaling molecules [13]. Therefore, it is vital for maintaining physiological homeostasis in cells. Furthermore, owing to its role in epithelial–mesenchymal transition and angiogenesis, CD44 has garnered attention as a potential therapeutic target for cancer [14]. Studies have revealed that CD44 participates in the pathophysiology of conditions such as diabetes, obesity, and other metabolic diseases by regulating glucose and lipid metabolism homeostasis [15,16]. Recently, researchers have reported that CD44 attenuates CCL4-induced acute liver injury by inhibiting ferroptosis [17]. Furthermore, another study has revealed that CD44 inhibits ferroptosis in tumor cells by regulating SLC7A11, primarily through the enhancement of SLC7A11 stability [18]. Deng et al. [19] demonstrated that the inhibition of ferroptosis by CD44 activation accelerates the progression of hepatocellular carcinoma caused by the hepatitis B virus. Given the pivotal role of CD44 in regulating ferroptosis, there has been a growing interest in CD44-related research in the field of ferroptosis.

For thousands of years, the therapeutic effects of plants have been extensively researched and acknowledged by populations globally, until the advent of organic chemical medicines. In recent decades, natural botanicals and plant-derived compounds have garnered renewed attention owing to their enhanced physical functioning and decreased side effects in reasonable doses [20]. At present, many plant-derived compounds that can improve the symptoms and prognosis of various diseases by modulating ferroptosis have been identified [21]. Platycodin D is a pentacyclic triterpenoid saponin isolated from the traditional Chinese medicine *Platycodon grandiflorum*. Both *in vivo* and *in vitro* experiments have revealed that this compound exhibits protective effects, including antioxidant, anti-inflammatory, and anticancer effects [22]. Recently, a study has revealed the capability of platycodin D for treating diabetic nephropathy by inhibiting ferroptosis in renal tubular cells [23]. Nevertheless, the therapeutic efficacy of platycodin D in treating PCOS remains unclear.

In the present study, we elucidated the role of CD44 in controlling the ferroptosis of GCs in PCOS. For this, we performed biochemical, clinical, and animal specimen analyses. Furthermore, using drug screening, the natural plant compound platycodin D was targeted. Lastly, through *in vivo* and *in vitro* experiments, we presented the effect of platycodin D in targeting CD44 to alleviate ferroptosis of GCs and thereby ameliorate PCOS.

2. Material and methods

2.1. Clinical samples

This study was conducted at Wuhan University's Renmin Hospital and included 42 patients with PCOS and 51 healthy women (as controls) who were undergoing *in vitro* fertilization and embryo transfer. The Ethics Committee of Wuhan University's Renmin Hospital approved this study (No. WDRY2019-K077). The PCOS diagnostic criteria were based on the 2003 Rotterdam criteria. Supplementary Table 1 summarizes the basic characteristics of the study participants. Using a previously described protocol, human ovarian GCs were obtained from the follicular fluid of patients.

2.2. Animal model

Three-week-old female Sprague Dawley rats were used to prepare the animal model. Dehydroepiandrosterone (DHEA, MedChemExpress, Shanghai, China) (6 mg/100 g body weight, dissolved in corn oil) was subcutaneously injected daily into rats with PCOS. In contrast, corn oil (MedChemExpress) was daily injected into control rats. From the 11th day, vaginal exfoliated cells were collected, smeared, and stained with methylene blue, followed by observation under a light microscope to determine the rat's estrous cycle. Injections were continued for 21 days. Thereafter, blood samples were collected from the inferior vena cava of rats. Rats were then sacrificed, and the ovaries were bilaterally collected. One part of the ovarian tissue was embedded with paraffin and sectioned, whereas the other part was frozen at −80 °C and used for subsequent experiments.

To elucidate the therapeutic effects of platycodin D *in vivo*, rats were divided into four groups: control, platycodin D, PCOS, and PCOS + platycodin D groups. The control and PCOS groups were treated as described previously. The rats in the platycodin D and PCOS + platycodin D groups were daily administered a platycodin D (MedChemExpress) solution (7.5 mg/kg) prepared using purified water. The rats in the other two groups were daily administered purified water.

In *in vivo* experiments to elucidate the effects of platycodin D on CD44 and SLC7A11, the rat ovaries were exposed by making an incision of approximately 3 cm on the back of the rats. Then, SLC7A11 and CD44 knockdown lentivirus or control virus (WZBio, Shandong, China) were injected into the rat ovaries in the four loci of the ovaries, followed by suturing the skin of the back of the rats for closure as we described previously [24]. After 5 days, the rats were divided into the following groups for modeling: control, PCOS, and PCOS + platycodin D groups.

2.3. Serum testosterone test

The Testosterone ELISA kit (Xinfan Biotech, Shanghai, China) was used to measure serum androgen levels.

2.4. Morphological observation of the ovary

Paraffin-embedded ovarian sections were hydrated and subsequently stained with hematoxylin–eosin stain (Servicebio, Wuhan, China), followed by sealing with resin. The sinus follicles, corpora lutea, and

vesicles were observed and counted under a light microscope.

2.5. Cell culture and transfection

The immortalized human ovarian GC line KGN was purchased from ATCC. Cells were cultured in DMEM F12 medium (Gibco, NE, US) supplemented with 10 % fetal bovine serum (Pernoside. Wuhan, China) and 200 μg/mL penicillin and streptomycin mixture (Gibco) in DMED/F12 medium (Gibco) at 37 °C under 5 % CO_2 conditions.

KGN cells were treated with 500 nM dihydrotestosterone (DHT) (Glpbio, Montclair, US) for 24 h to establish an *in vitro* PCOS model. To explore the effect of platycodin D, KGN cells were treated with 10 μM platycodin D for 24 h.

To knock down CD44 or SLC7A11 expression, KGN cells were first cultured until 70 % confluency. Then, Lipofecamine 2000 (Thermo Fisher, 11668019) was used to transfect cells with CD44 siRNA(WZ biosciences, Shandong, China), si-SLC7A11 (WZ biosciences), and control si RNA (WZ biosciences).

2.6. Quantitative polymerase chain reaction (qPCR)

A previously described method was utilized to measure mRNA expression [25]. Supplementary Table 2 lists the relevant primer sequences. The data were transformed using the $2^{-\Delta\Delta Ct}$ method.

2.7. Molecular docking

The protein structures of CD44 (ID: P16070) and SLC7A11 (ID: Q9UPY5) were downloaded from UniProt. The structures of small molecules such as platycodin D were downloaded from PubChem. The small molecules were assigned as ligands and the proteins as receptors. After performing docking using Vina, the scores of protein–small molecule combinations were calculated. Then, Pymol and Discovery Studio software (version 4.3.0) were utilized to analyze and visualize the forces in three-dimensional (3D) and two-dimensional (2D) angles. Ligplus software was utilized to map the amino acid residues interacting between two proteins in 3D and 2D angles.

2.8. Molecular dynamics simulation

The kinetic simulation software was Gromacs 2018. An all-atom explicit solvent model of the platycodin D-CD44 protein complex was established. The simulation temperature was 300K and the time was 100 ns. Amber99sb-ildn was utilized as the protein and small molecule force field, and TIP3P was used as the water model. The size of the system box was $10 \times 10 \times 10$ nm^3 and the minimum distance between the complex and the system box was 1 nm.

The energy was minimized using the steepest descent method, with a maximum number of steps of 50,000. The cutoff distances of Coulomb force and van der Waals radius were 1 nm. The normal variable–temperature (NVT) and isothermal–isoparaffinic (NPT) systems were used to equilibrate the system. Molecular dynamics was performed at ambient temperature and pressure. The built-in analysis module of Gromacs2018 was used to perform data analysis of the simulated trajectories. Root mean square deviation (RMSD) was utilized to observe the overall conformational changes in the proteins of the system compared with the initial structure during the simulation. The tightness of the system structure was evaluated using the radius of gyration. Structural fluctuations in the local amino acid residue sites of the system during the simulation process were observed using root mean square fluctuation (RMSF).

2.9. Western blotting

Previously described methods were used to perform total protein extraction from tissues and cells and western blotting [24]. The membranes containing proteins were incubated with the following primary antibodies at 4 °C for 16 h: CD44(Proteintech, 15675-1-AP, 1:1000), SLC7A11(Abcam, ab307601, UK, 1:1000), GPX4 (Proteintech,67763-1-Ig, 1:1000), FTH1 (Proteintech,11682-1-AP 1:1000), TFR1 (Proteintech,10084-2-AP,1:2000), and ACTB (Proteintech, rabbit, 81115-1-RR 1:5000). Subsequently, the strips were washed with Tris-buffered saline with Tween 20 (TBST) and incubated with horse radish peroxidase (HRP)-conjugated secondary antibody for 2 h. The strips were then washed with TBST and quantitatively observed using the Bio-Rad ChemiDocTM XRS + System.

2.10. Co-immunoprecipitation (Co-IP) assay

As previously described, KGN cell lysis buffer was used to extract proteins [24]. Briefly, the supernatants of the cell lysate were combined with 5 μL of primary antibody and 40 μL of protein A + G agarose suspension beads. (Santa Cruz, Dallas, Texas, USA), followed by incubation at 4 °C overnight. Subsequently, the beads were rinsed with lysate and the samples were boiled at 100 °C for 5 min. Finally, western blotting was performed.

2.11. Cellular thermal shift assay (CETSA)

KGN cells were collected, and the lysates were treated with a protease inhibitor. Subsequently, the cell lysate was divided into two parts and incubated with platycodin D solution and dimethyl sulfoxide, respectively, for 2 h at room temperature. Then, the lysates were homogenized and treated for 3 min at 37 °C, 42 °C, 47 °C, 52 °C, 57 °C, 62 °C, 67 °C, and 72 °C. The samples were placed on ice for cooling, followed by western blotting.

2.12. Biochemical detection

Approximately 10 mg of ovarian tissue was collected from each group, washed with pre-cooled phosphate-buffered saline (PBS), and homogenized. An ultrasonic cell fragmentation system was used to homogenize KGN cells. Fe^{2+} levels were measured in cells and tissues using the Ferrous Ion Content Assay Kit (Dojindo, I291, Japan). The absorbance was measured at 593 nm to determine Fe^{2+} levels. Glutathione (GSH) levels were measured in tissues and cells using a Glutathione assay kit (Solarbio, BC1175). The absorbance was measured at 412 nm. Malondialdehyde (MDA) levels were measured using the MDA Assay Kit (Nanjing Jiancheng Bio-Engineering Institute, #A003-1). The absorbance was measured at 535 nm.

2.13. Immunofluorescence staining

Paraffin-embedded ovarian sections were dewaxed and hydrated. KGN cells were fixed with paraformaldehyde. Membranes were ruptured using 0.3 % Triton (Solarbio, #T8200, China), followed by the antigenic closure of cells and sections using goat serum. After 30 min, the cells were incubated with primary antibodies against CD44, SLC7A11, and FSHR (Proteintech, 22665-1-AP) at 4 °C. The next day, tissue sections and cells were washed with TBST, followed by incubation with Cy3-labelled and FITC-labelled secondary antibodies for 1 h at room temperature. 4′,6-Diamidino-2-phenylindole (DAPI) was used to stain the cell nuclei. Images were captured using a microscope (Olympus, BX53, Japan).

2.14. Immunohistochemical staining

Paraffin-embedded ovarian sections were dewaxed and hydrated. Then, the membrane was ruptured using 0.3 % Triton. The samples were incubated with 10 % H_2O_2 for 20 min, followed by the antigenic closure of cells and sections using goat serum. After 30 min, the samples were incubated with primary antibody against 4HNE (R&D Systems,

MAB3249, 1:200) at 4 °C overnight. Then, the sections were washed with TBST and incubated with HRP-conjugated Goat Anti-Mouse IgG (H + L) for 1 h. 3, 3′-Diaminobenzidine staining was performed for color development. The cell nuclei were stained with DAPI, followed by sealing. Images were captured using a microscope (Olympus, BX53, Japan).

2.15. Transmission electron microscopy

Fresh ovarian tissues measuring 2 mm^3 were collected and incubated with an electron microscope fixative for 5 h. Subsequently, samples were fixed with 0.1 M PBS with 1 % osmium acid for 2 h at room temperature. After washing the samples with PBS, they were dehydrated using a gradient of 50%–100 % alcohol. Then, samples were permeabilized using 100 % acetone. Subsequently, the samples were dried in an oven at 60 °C and sectioned using an ultrathin slicer (Leica, Switzerland). Sections were stained with uranium lead. Images were captured under a projection electron microscope (Hitachi, Japan) and analyzed.

2.16. Reactive oxygen species (ROS) detection

A 1 μM solution of the superoxide anion fluorescent probe dihydroethidium (DHE, Beyotime, S0063) was dropped on tissue sections, followed by incubation for 30 min in the dark. The cell nuclei were stained with DAPI, followed by PBS washing. The images were captured using a microscope.

Cells were incubated with 1 μM DHE solution for 30 min in the dark and subsequently washed with PBS. An inverted microscope (Olympus IX73P2F, Japan) was used for observation.

MitoSOX dye (Thermo Fisher, M36008) was used to detect mitochondrial ROS. First, cells were washed with PBS; then, they were incubated with 1 mL of 5 μM MitoSOX dye for 30 min in the dark, followed by washing three times with PBS. A confocal microscope (Olympus, Japan) was used to collect the images.

2.17. MitoTracker red staining

Cells were incubated with 50 nM MitoTracker Red (Yeasen, China) for 20 min, and then sealed with Hoechst 33342 Staining Solution (Beyotime, C1027) for 10 min, followed by washing three times with PBS. A confocal microscope (Olympus, Japan) was used to collect the images.

2.18. Lipid detection

Lipid marking of cells was performed using BODIPY™ 493/503 C11 (Thermo Fisher, D3922, Waltham, US). First, the cells were fixed with paraformaldehyde. Then, they were incubated with an appropriate amount of staining solution for 20 min in the dark, followed by washing with PBS. The cells were observed under a microscope.

2.19. GST pull down

The E. coli cells were transfected with GST-CD44 and His-SLC7A11 (WZ biosciences), and the fusion proteins were obtained as previously described by other authors [26]. Approximately 100 μg of GST and GST-CD44 fusion proteins were immobilized in GSTSep Glutathione MagBeads (Yeasen, 20562ES03, Shanghai) and incubated for 120 min at room temperature. Then, beads were washed three times with washing buffer. Subsequently, 100 μg of His-SLC7A11 was added to GST and GST-CD44, respectively, and the samples were incubated overnight at 4 °C. The bound proteins were then eluted using elution buffer and Western blot for analysis.

2.20. Statistical analysis

GraphPad Prism 9 software was used for data analysis. All quantitative data are expressed as mean ± standard deviation. Student's two-tailed *t*-test was performed to establish the statistical significance of the two groups. Multiple comparisons were analyzed using one-way analysis of variance, followed by Tukey's post hoc test. A P-value of <0.05 was considered statistically significant.

3. Results

3.1. Increased GC ferroptosis in patients with PCOS and DHEA-treated rats

Previous studies have revealed that ferroptosis plays a role in PCOS pathogenesis [27]. Therefore, to investigate whether ferroptosis participates in the damage of PCOS GCs, we collected GCs from the follicular fluid of patients with PCOS and healthy controls undergoing *in vitro* fertilization and embryo transfer and measured the mRNA expression of ferroptosis-related genes (Fig. 1A). The mRNA expression of ferroptosis-related molecules, namely, SLC7A11, GPX4, and FTH1, was significantly lower in the GCs of patients with PCOS than in those from control patients (Fig. 1B); in contrast, the mRNA expression of TFR1 was significantly higher (Fig. 1B). Furthermore, western blotting revealed an increase in the protein levels of SLC7A11, GPX4, and FTH1 but a decrease in TFR protein levels in the GCs of PCOS patients with PCOS (Fig. 1C and D). These findings suggest the presence of ferroptosis in the GCs of patients with PCOS.

Next, we measured the mRNA and protein levels of ferroptosis-regulating molecules in DHEA-treated rats. The results were consistent with the expression of ferroptosis-related molecules in the GCs of patients with PCOS (Figure E–G). Subsequently, the levels of 4HNE, a lipid peroxidation product, were examined in rat ovaries. Immunohistochemical analysis revealed that 4HNE levels were significantly higher in the ovarian GCs of rats with PCOS than in those of control rats (Fig. 1H and I). In addition, the level of GSH in GCs was significantly lower in rats with PCOS compared to controls. Conversely, the levels of MDA and Fe^{2+} were lower than in control rats (Fig. 1J–L). These findings suggest that the involvement of ferroptosis in PCOS pathogenesis.

3.2. CD44 is a key regulatory molecule for GC ferroptosis in PCOS

To identify the key regulatory molecules associated with ferroptosis in PCOS, the GEO dataset was searched. This dataset had been previously sequenced to obtain the RNA of GCs from patients with PCOS (GEO accession number: GSE155489). As a result, 1034 differentially expressed genes (DEGs) were identified from the GCs of the patients in the control and PCOS groups (Fig. 2A). Kyoto Encyclopedia of Genes and Genomes enrichment analysis revealed that the DEGs are primarily involved in ferroptosis, mitochondrial autophagy, and other related pathways (Fig. 2B). From these, we selected the regulatory molecules associated with ferroptosis and established a heat map (Fig. 2C). Furthermore, correlation analysis demonstrated that CD44 was correlated with key genes that regulate ferroptosis in GCs, including SLC7A11, SLC3A2, ACSL4, etc. (Fig. 2D). Notably, CD44 was significantly downregulated in the PCOS group. Subsequently, we validated this finding in the GCs of patients with PCOS and observed that the mRNA and protein levels of CD44 were also significantly downregulated in the GCs of patients with PCOS (Fig. 2E–G). In addition, correlation analysis showed that CD44 expression was significantly negatively correlated with ovarian function indicators(Fig. 2H–K),such as antral follicle count (AFC) ($r = -0.3839$, $p = 0.0138$), body mass index (BMI) ($r = -0.5409$, $p = 0.0018$), anti-Mullerian hormone (AMH) ($r = -0.3904$, $p = 0.0128$), and serum testosterone levels ($r = -0.3083$, $p = 0.0317$). These findings suggest the potential role of CD44 in PCOS pathogenesis and its association with ferroptosis.

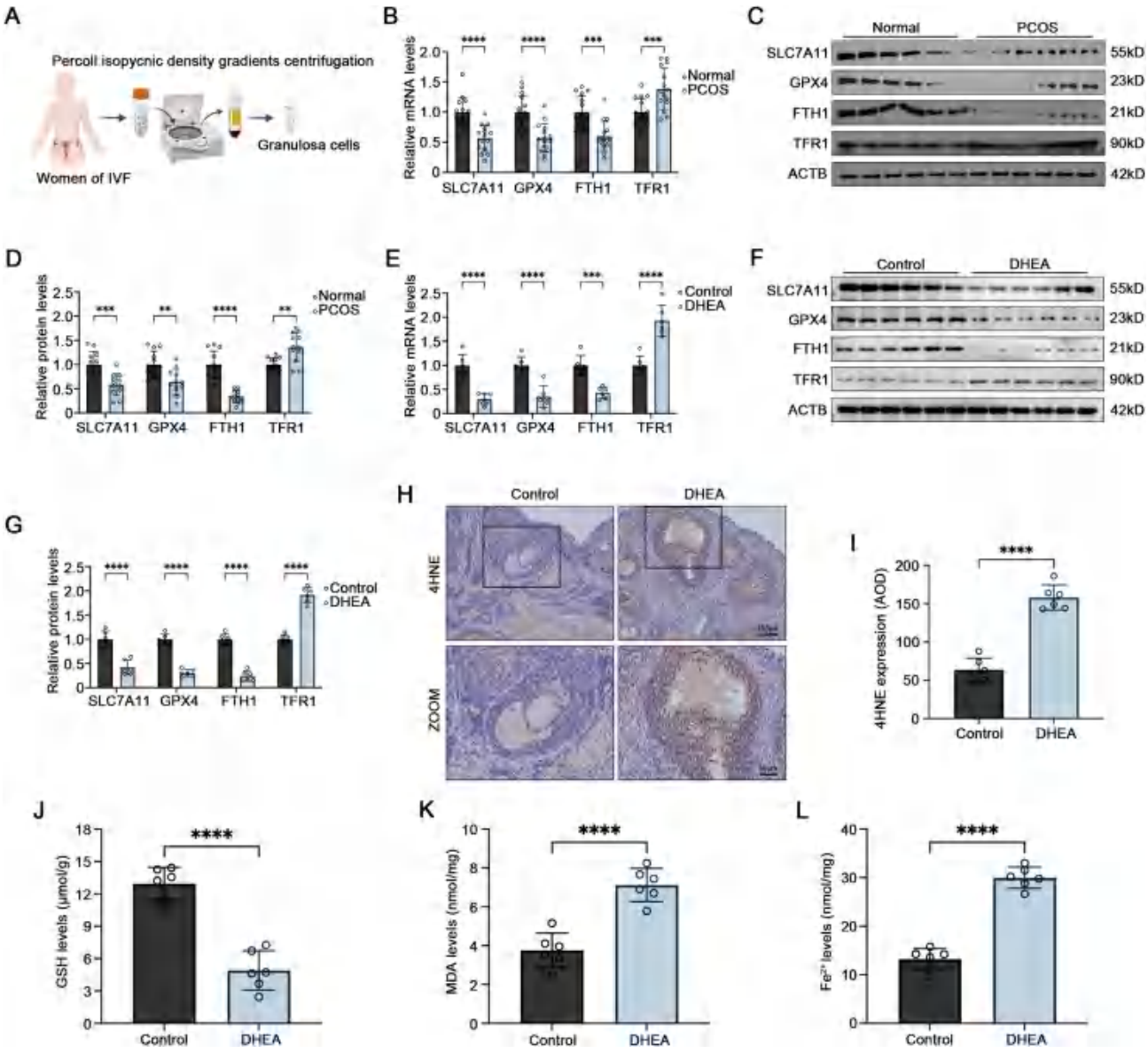

Fig. 1. Elevated levels of ferroptosis in granulocytes in PCOS patients and animal models
A. Procedure for human granulosa cells collection. B. Quantification of the mRNA level of SLC7A11, GPX4, FTH1 and TFR1 in PCOS patients and healthy control women (n = 15). C, D. Quantification of the protein level of SLC7A11, GPX4, FTH1 and TFR1 in PCOS patients and healthy control women (n = 12). E. Quantification of the mRNA level of SLC7A11, GPX4, FTH1 and TFR1 in DHEA-treated rats and controls (n = 6). F, G. Western blot and densitometric analysis for the expression of SLC7A11, GPX4, FTH1 and TFR1 in DHEA-treated rats and controls. (n = 6). H, I. Immunohistochemical analysis of 4HNE expression in PCOS rats with controls (n = 6). J-L. Levels of GSH, Fe^{2+} and MDA in rat ovarian tissue (n = 6). Data are presented as mean ± SD. Student's t-test. **p < 0.01; ***p < 0.001; ****p < 0.0001.

3.3. Drug screening to alleviate ferroptosis by targeting CD44

Recently, studies have revealed the capacity of natural plants and their extracts to alleviate ferroptosis in various diseases [21,28]. To identify the botanical drugs that alleviate ferroptosis in PCOS, we screened the botanical drugs that can improve ferroptosis in different diseases; as a result, we identified 19 drug candidates (Supplementary Table 3) Next, to identify the potential drugs targeting CD44, the 20 drug candidates and CD44 were subjected to molecular docking simulations. Based on the simulation results, the top five drugs with the best binding energies were selected (Supplementary Fig. 1). Subsequently, we performed the cell viability assay to determine the appropriate concentrations of these five drugs in the human immortalized GC line KGN (Supplementary Fig. 2). Then, KGN cells were treated with each drug to measure CD44 protein levels. Western blotting revealed that CD44 protein levels were the most significantly elevated in platycodin D-treated KGN cells (Fig. 2L and M). Furthermore, CETSA revealed higher CD44 stability in platycodin D-treated KGN cells (Fig. 2N and O). Besides, the time evolution of RMSD and Rg in molecular dynamics simulations demonstrated that both CD44 and platycodin D reached equilibrium within 100 ns simulations, and the system stabilised and converged (Fig. 2P–S). The sites of action of CD44 and Platycodin D were identified in the region of the first 200 amino acids. The RMSF values of the first 200 amino acids of the proteins in both systems were found to be less than 1 nm, with only minor fluctuations (Fig. 2T). Additionally, the three-dimensional free energy surface map can be used to reflect the conformational energy distribution of the protein in the simulation. The energy of the overall conformation of CD44 binding to platycodin D is relatively high, and after performing the equilibrium simulation for a period of time, a structure located at the global energy minimum can be observed (Fig. 2U). Consequently, in subsequent studies, platycodin D was used to improve ferroptosis.

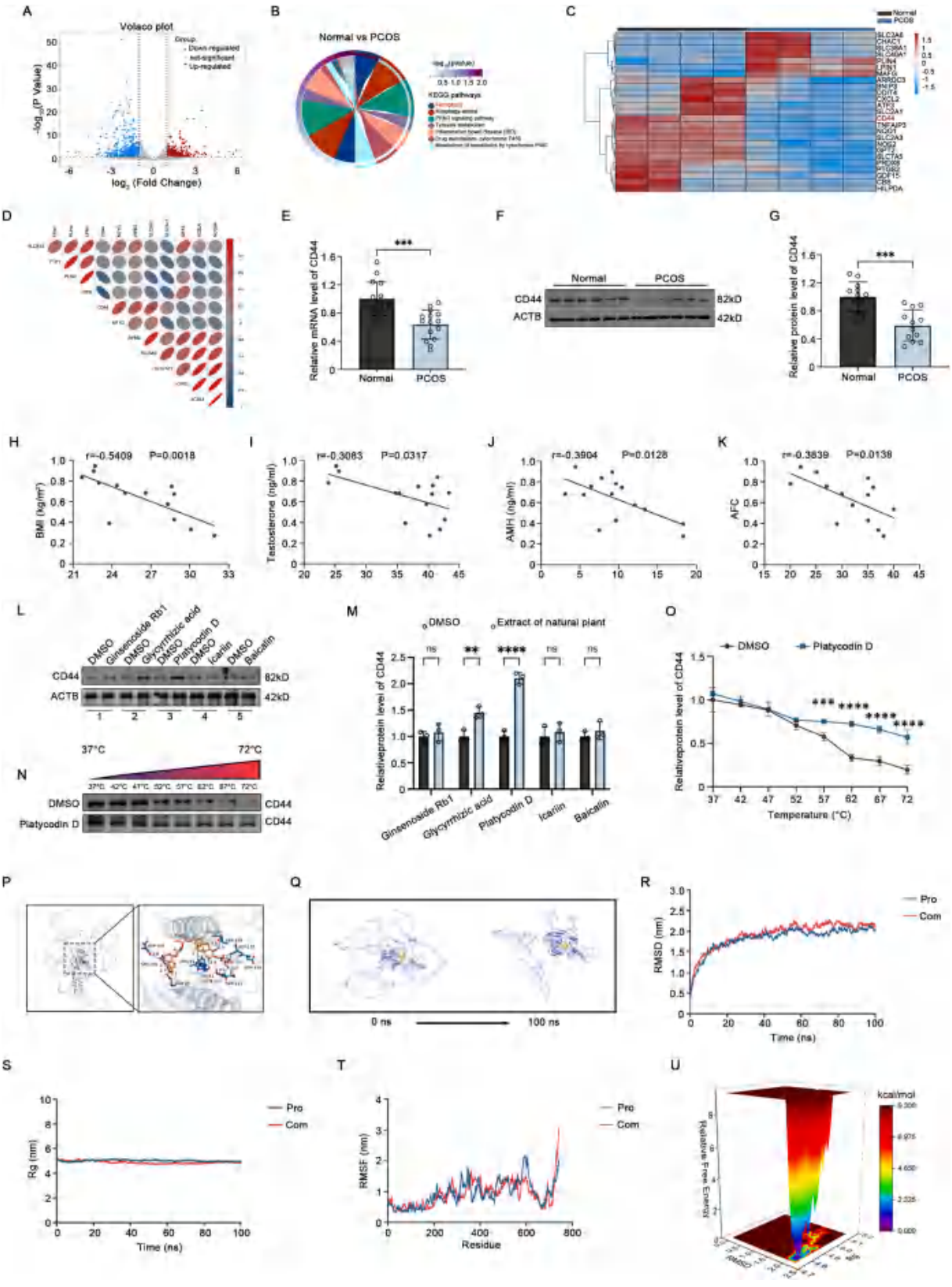

(caption on next page)

Fig. 2. Drug screening for alleviation of ferroptosis in PCOS by targeting CD44
A. Volcano plot of gene expression changes in the PCOS ovaries versus control (n = 4). B. KEGG enrichment analyses. C. Heatmap of ferroptosis related molecule expression in the DEGs. D. Correlation analysis of the genes associated with ferroptosis. E. Quantification of the mRNA level of CD44 in PCOS patients and healthy control women (n = 15). F, G. Western blot and densitometric analysis for the expression of c CD44 in PCOS patients and healthy control women (n = 12). H-K. Association of CD44 expression with AFC, BMI, Testosterone, and AMH. L, M. Effects of natural plant extracts on CD44 on protein levels (n = 3). N, O. Western blot showed the effect of platycodin D on the thermal stability of CD44 (n = 3). P. Representative images of the docking mode of Platycodin D binding to CD44. Q. The trajectory changes of platycodin D-CD44 complex from 0 s to 100 s. R. RMSD was utilized to observe the overall conformational changes in the proteins of the system compared with the initial structure during the simulation. S. Rg was used to evaluate the tightness of the system structure. T. RMSF was used to evaluate the structural fluctuations of local amino acid residue sites of the system during the simulation process. U. Three-dimensional free energy surface maps reflect the conformational energy distribution of cs44 in simulations. Data are presented as mean ± SD. Student's t-test. **p < 0.01; ***p < 0.001; ****p < 0.0001. ns, not significant.

3.4. Platycodin D attenuates disorders of the estrous cycle, high androgen levels, and abnormal follicular development in rats with PCOS

To investigate the potential therapeutic effect of platycodin D on PCOS, a PCOS rat model was established by subcutaneously injecting DHEA. Then, platycodin D was orally administered to intervene in the model (Fig. 3A). The optimal platycodin D concentration for treating rats with PCOS was determined to be 7.5 mg/kg via a preliminary experiment (Supplementary Fig. 3). During the modeling period, the body weights of the rats were recorded. DHEA-treated rats exhibited a significantly higher body weight compared with control rats; however, platycodin D-treated rats with PCOS exhibited significantly decreased body weight (Fig. 3B). Furthermore, serum testosterone levels were significantly higher in rats with PCOS than in control rats; however, treatment with platycodin D partially restored testosterone levels in rats with PCOS (Fig. 3C). Subsequently, vaginal exfoliated cells were stained with methylene blue to determine the estrous cycle (Fig. 3D and E). Staining revealed the disruption of the estrous cycle and prolongation of

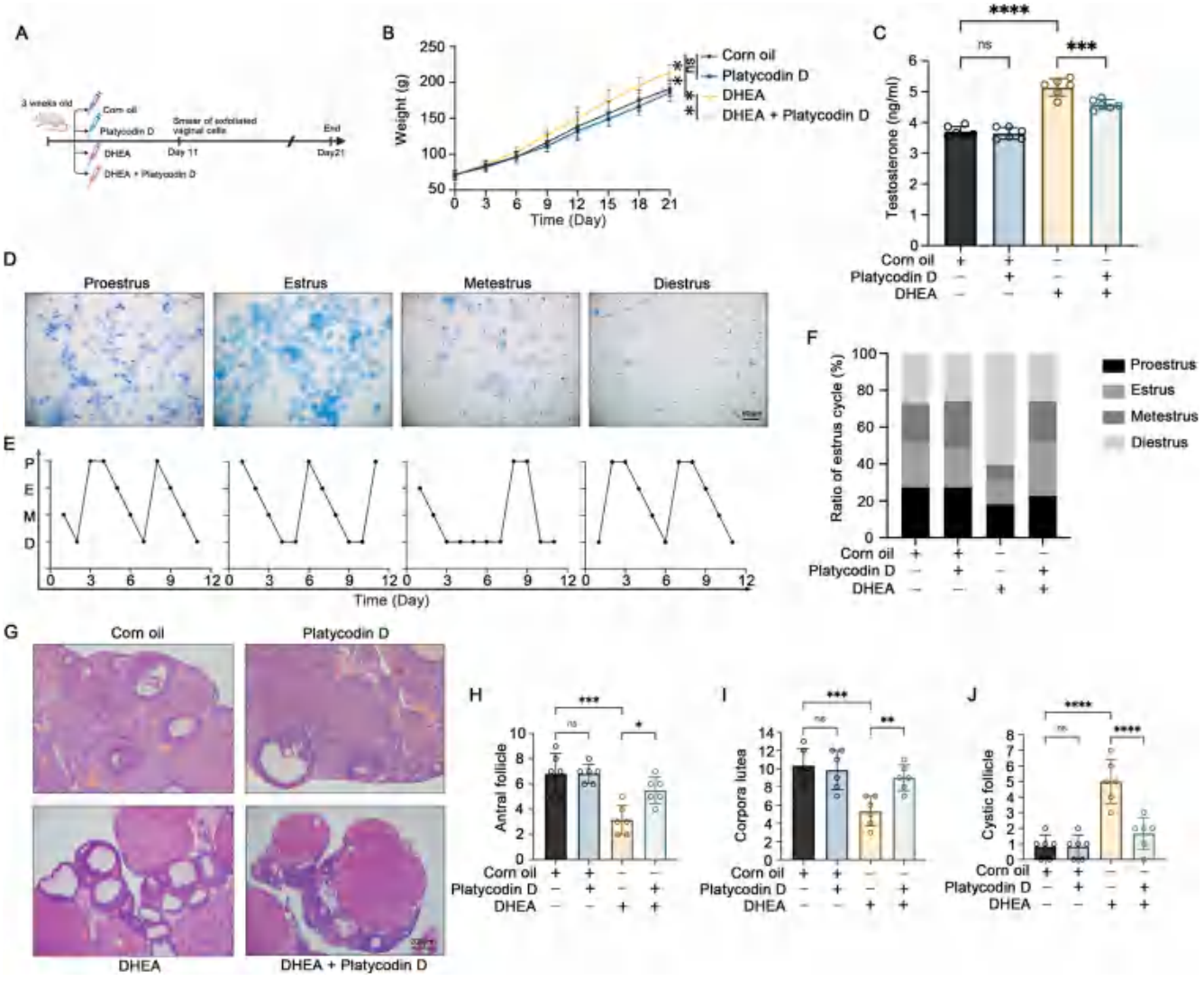

Fig. 3. Platycodin D attenuates disorders of the estrous cycle, high androgen levels and abnormal follicular development in PCOS rats
A. Schematic diagram of the treatment of platycodin D in PCOS rats. B. Effect of platycodin D on body weight in PCOS rats (n = 6). C. The level of serum testosterone in rats (n = 6). D. Methylene blue staining of smears of rat vaginal exfoliated cells. E, F. Estrous cycle status in rats (n = 6). G. Pathological observation of ovary in rats. H-J. The number of antral follicles, corpora lutea and cystic follicles in each group was statistically analyzed. (n = 6). one-way ANOVA. *p < 0.05; **p < 0.01; ***p < 0.001; ****p < 0.0001; ns, not significant.

the inter-estrous period in rats with PCOS. In contrast, treatment with platycodin D partially restored the estrous period in rats with PCOS (Fig. 3F). Furthermore, histological examination of the ovaries of rats with PCOS revealed a significant reduction in the sinus follicles and corpora lutea, but an increase in the number of cystic follicles compared with the control group. Platycodin D treatment significantly decreased the cystic follicles and increased the sinus follicles and corpora lutea in the ovaries of rats with PCOS (Fig. 3G–J). Collectively, these findings suggest the beneficial effect of platycodin D on increased body weight, disrupted estrous cycles, increased androgen levels, and aberrant follicular development in rats with PCOS.

3.5. Platycodin D attenuates ferroptosis in rats with PCOS

Our goal was to investigate the effect of platycodin D on ferroptosis in PCOS. For this, we measured 4HNE levels in the rat ovaries. Immunohistochemical staining revealed that 4HNE levels were significantly higher in the ovaries of rats with PCOS than in those of control rats. Furthermore, platycodin D treatment significantly decreased 4HNE levels in the ovaries of rats with PCOS (Fig. 4A and B). Subsequently, a DHE probe was used to measure ROS levels in the rat ovaries. ROS levels were significantly higher in the PCOS group than in the control group. However, platycodin D treatment decreased ROS levels in the ovaries of rats with PCOS (Fig. 4C and D). Transmission electron microscopy revealed vacuolization in the mitochondria in the ovarian tissues of DHEA-treated rats, the disordered arrangement of the mitochondrial cristae, and the absence of membrane integrity. In contrast, following platycodin D treatment, the rats exhibited effective improvements in mitochondrial morphology and structural integrity (Fig. 4E and F). Subsequently, we performed immunofluorescence staining to examine CD44 levels in the rat ovaries. CD44 levels were significantly decreased in GCs in the ovaries of DHEA-treated rats. In contrast, following treatment with platycodin D, CD44 levels were partially restored in the GCs of rats with PCOS (Fig. 4G and H). Subsequently, we measured MDA and Fe^{2+} levels in rat ovarian tissues, which are essential products of oxidative stress and ferroptosis, respectively. We observed that MDA and Fe^{2+} levels were significantly higher in rats with PCOS than in control rats. However, they were significantly restored in the ovaries of rats with PCOS treated with platycodin D (Fig. 4I and J). Furthermore, GSH levels were significantly decreased in the ovaries of rats with PCOS; the levels were partially restored in platycodin D-treated rats (Fig. 4K). Western blotting revealed a significant decrease in the protein levels of CD44, SLC7A11, FTH1, and GPX4 but an increase in the levels of TFR1 in the ovaries of rats with PCOS compared with those of control rats. In addition, treatment partially restored the protein levels of CD44 and SLC7A11 in the ovaries of rats with PCOS; however, no significant effect was observed on the levels of FTH1, GPX4, and TFR1 (Fig. 4L and M). Collectively, these results provide preliminary evidence that platycodin D can alleviate GC ferroptosis in the ovaries of rats with PCOS. This therapeutic effect may be associated with CD44 and SLC7A11 activation.

3.6. Platycodin D ameliorates DHT-induced ferroptosis in GCs and KGN cell line

To further confirm the ameliorating effect of platycodin D on GC ferroptosis in PCOS, we treated KGN cells with DHT to mimic the hyperandrogenic environment and then administered platycodin D. Initially, the impact of platycodin D on mitochondrial fission in KGN cells was examined. DHT treatment led to the formation of fragmented, punctate mitochondria, whereas platycodin D treatment demonstrated a capacity to mitigate these alterations in mitochondrial structure(Fig. 5A and B). Bodipy dye was used to detect the lipid accumulation status in KGN cells. Staining revealed significant lipid accumulation in DHT-treated cells. However, platycodin D administration decreased lipid accumulation in KGN cells in a hyperandrogenic environment (Fig. 5C and D). Furthermore, DHT treatment markedly increased MDA levels in KGN cells; however, platycodin D administration partially decreased MDA levels in KGN cells (Fig. 5I). These results suggest that platycodin D significantly attenuates lipid peroxidation in KGN cells under hyperandrogenic conditions. Furthermore, DHE probe staining revealed a higher ROS content in the DHT group than in the control group; however, platycodin D decreased ROS production in KGN cells (Fig. 5E and F). Next, mitochondrial ROS levels were detected via MitoSOX staining. Mitochondrial ROS was significantly higher in DHEA-treated KGN cells; however, platycodin D decreased mitochondrial ROS accumulation (Fig. 5G and H). Furthermore, platycodin D partially revered the hyperandrogenism-induced increase in Fe^{2+} levels in KGN cells (Fig. 5J). In addition, platycodin D significantly restored the DHT-induced decrease in GSH levels (Fig. 5K). Immunofluorescence staining revealed a significant decrease in CD44 levels in DHT-treated KGN cells; however, platycodin D partially restored CD44 levels (Fig. 5L and M). Subsequently, we measured the protein levels of ferroptosis-related proteins and observed that androgen significantly decreased the protein levels of CD44, SLC7A11, GPX4, and FTH-1 but increased those of TFR1 in KGN cells. Nevertheless, platycodin D treatment partially restored CD44 and SLC7A11 levels and did not significantly affect the expression of the remaining molecules; this was consistent with the results obtained in in vivo experiments (Fig. 5N and O). Besides, we performed the same treatment on human GCs obtained from follicular fluid and found that PD exerts an anti-ferroptosis effect in primary GCs and activates the expression of CD44 and SLC7A11(Supplementary Fig. 4).

In a previous study on colorectal cancer, CD44 and SLC7A11 were identified as key molecules that interact and are involved in regulating ferroptosis [29]. Therefore, to determine whether CD44 and SLC7A11 interact with each other, we subjected these two molecules to molecular docking simulations. We observed that the amino acid residue 158 LYS of the CD44 protein binds to the amino acid residue 179 LEU of the SLC7A11 protein via a 3.0 Å hydrogen bond. Furthermore, both proteins can be bound by multiple cooked sleeper forces, resulting in the stable binding of both proteins (Fig. 5P). Next, we verified the interaction between the two molecules via Co-IP. The protein collected with the antibody against CD44 contained SLC7A11. Furthermore, the antibody against SLC7A11 captured the CD44 protein. Platycodin D enhanced the interaction between CD44 and SLC7A11 (Fig. 5Q and R). In addition, the GST-pull down results suggest that there appeared to be a weak binding between SLC7A11 and CD44 (Supplementary Fig. 5). Collectively, these results suggest that platycodin D attenuates hyperandrogenism-induced ferroptosis in KGN cells. This effect is associated with CD44 and SLC7A11 regulation.

3.7. Platycodin D alleviates ferroptosis in KGN cells by targeting CD44/SLC7A11

To elucidate the mechanism by which platycodin D alleviates ferroptosis in KGN cells, we transfected KGN using CD44 siRNA and examined the effect of platycodin D on ferroptosis in KGN under a hyperandrogenic environment. The siRNA with the highest knockdown efficiency was selected for subsequent silencing of target genes (Supplementary Figs. 6A–C). Immunofluorescence and western blotting assays revealed that SLC7A11 levels significantly increased in KGN cells transfected with empty RNA in a hyperandrogenic environment after treatment with platycodin D. Silencing CD44 inhibited the activation of SLC7A11 by platycodin D (Fig. 6A–E). Subsequently, we evaluated the levels of Fe^{2+} and MDA in KGN cells and found that the effect of Platycodin D in reducing Fe^{2+} and MDA in KGN cells was significantly attenuated after transfection with CD44 siRNA (Fig. 6F and G). Additionally, CD44 siRNA significantly inhibited the restoration of GSH by platycodin D (Fig. 6H). Furthermore, the capacity of platycodin D to diminish mitochondrial fragmentation was partially reversed by CD44 siRNA (Fig. 6I and J). Bodipy staining revealed that CD44 knockdown significantly inhibited the lipid scavenging effect of Platycodin D in KGN

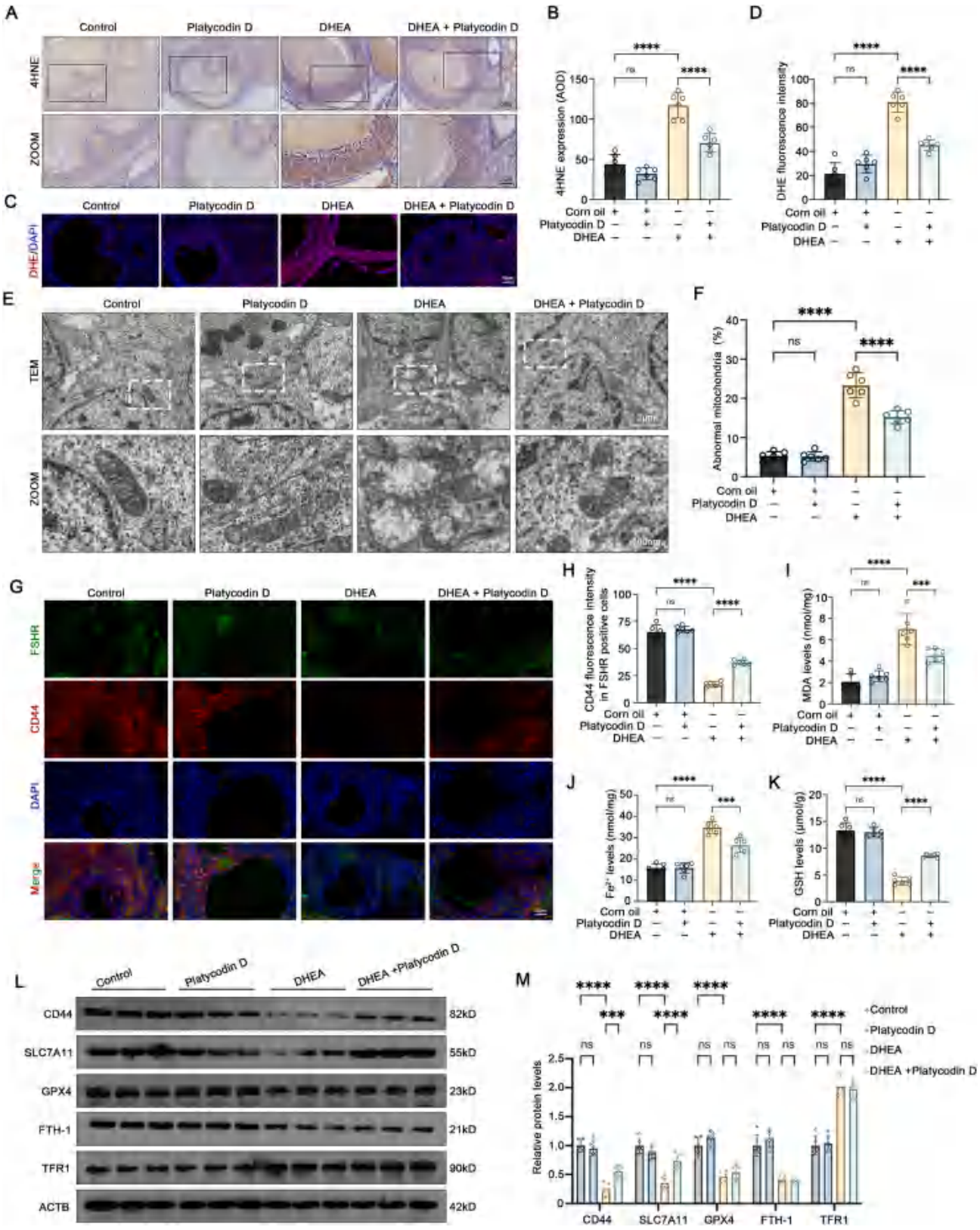

Fig. 4. Platycodin D attenuates ferroptosis in PCOS rats

A, B. Immunohistochemical analysis of 4HNE expression in the ovaries of rats (n = 6). C, D. ROS levels in ovarian tissue were detected using DHE probe (n = 6). E, F. Mitochondria of GCs in rat ovarian tissue were observed by TEM (n = 6). G, H. The levels of CD44 in rat ovarian GCs were detected by immunofluorescence staining (n = 6). I-K. MDA, Fe^{2+} and GSH levels in rat ovarian tissue (n = 6). L, M. Western blot and densitometric analysis for the expression of CD44, SLC7A11, GPX4, FTH1 and TFR1 in ovaries of the rats (n = 6). one-way ANOVA. ***p < 0.001; ****p < 0.0001; ns, not significant.

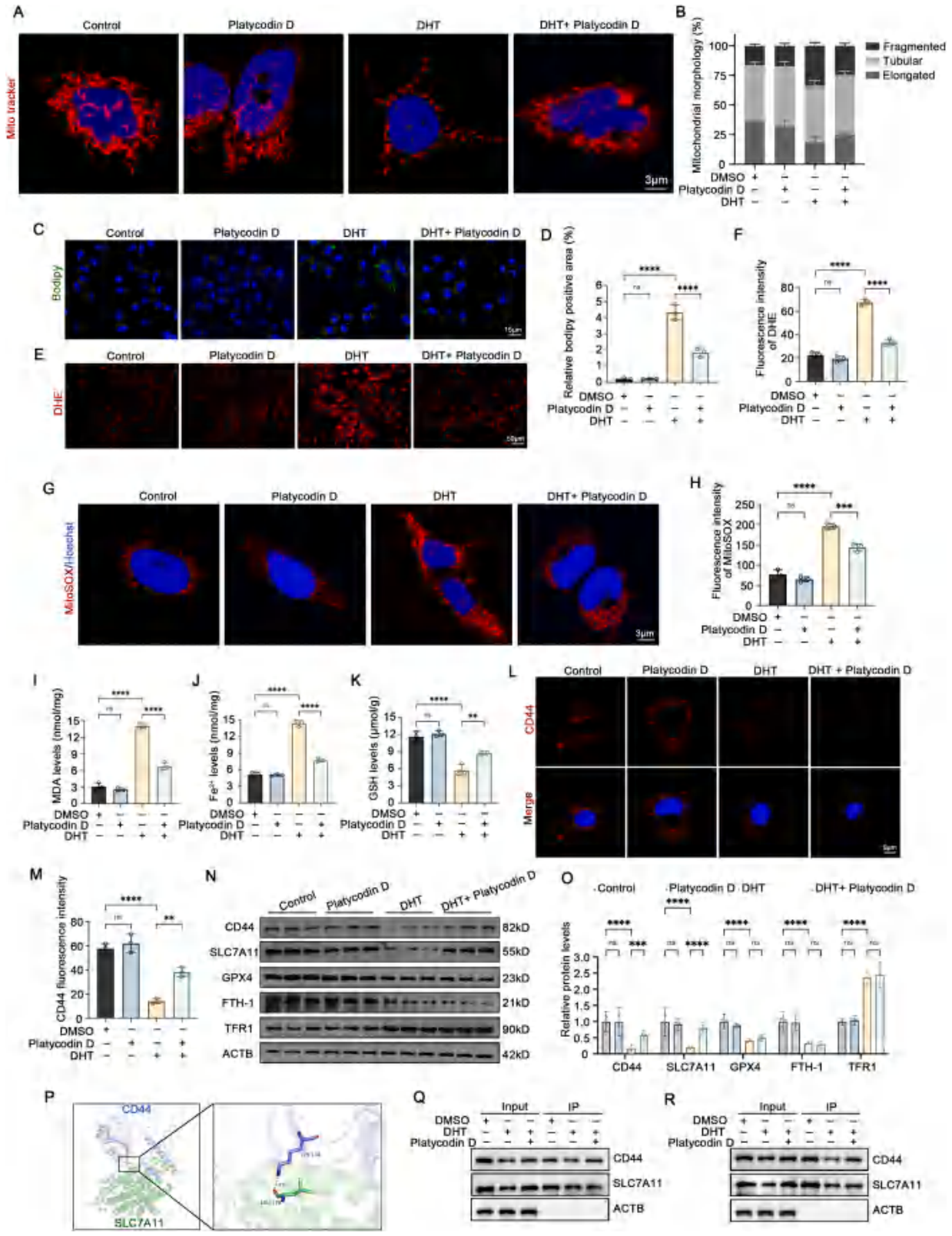

Fig. 5. Platycodin D ameliorates DHT-induced ferroptosis in KGN cells

A, B. Representative confocal microscopy image of MitoTracker Red staining in KGN cells (n = 3). C, D. Lipid accumulation in KGN cells was detected by BODIPY probe (n = 3). E, F. ROS levels in KGN cells were detected using DHE probe (n = 3). G, H. ROS levels of mitochondria in KGN cells were detected using MitoSOX probe (n = 3). I-K. MDA, Fe^{2+} and GSH levels in KGN cells (n = 3). L, M. The levels of CD44 in KGN cells were detected by immunofluorescence staining (n = 3). N, O. Western blot and densitometric analysis for the expression of CD44, SLC7A11, GPX4, FTH1 and TFR1 in KGN cells (n = 3). P. Molecular docking simulation of CD44 and SLC7A11. Q. Interaction between CD44 and SLC7A11 in KGN cells determined by CO-IP analysis using anti-CD44 antibodies. R. Interaction between CD44 and SLC7A11 in KGN cells determined by CO-IP analysis using anti-SLC7A11 antibodies. one-way ANOVA. **p < 0.01; ***p < 0.001; ****p < 0.0001; ns, not significant.

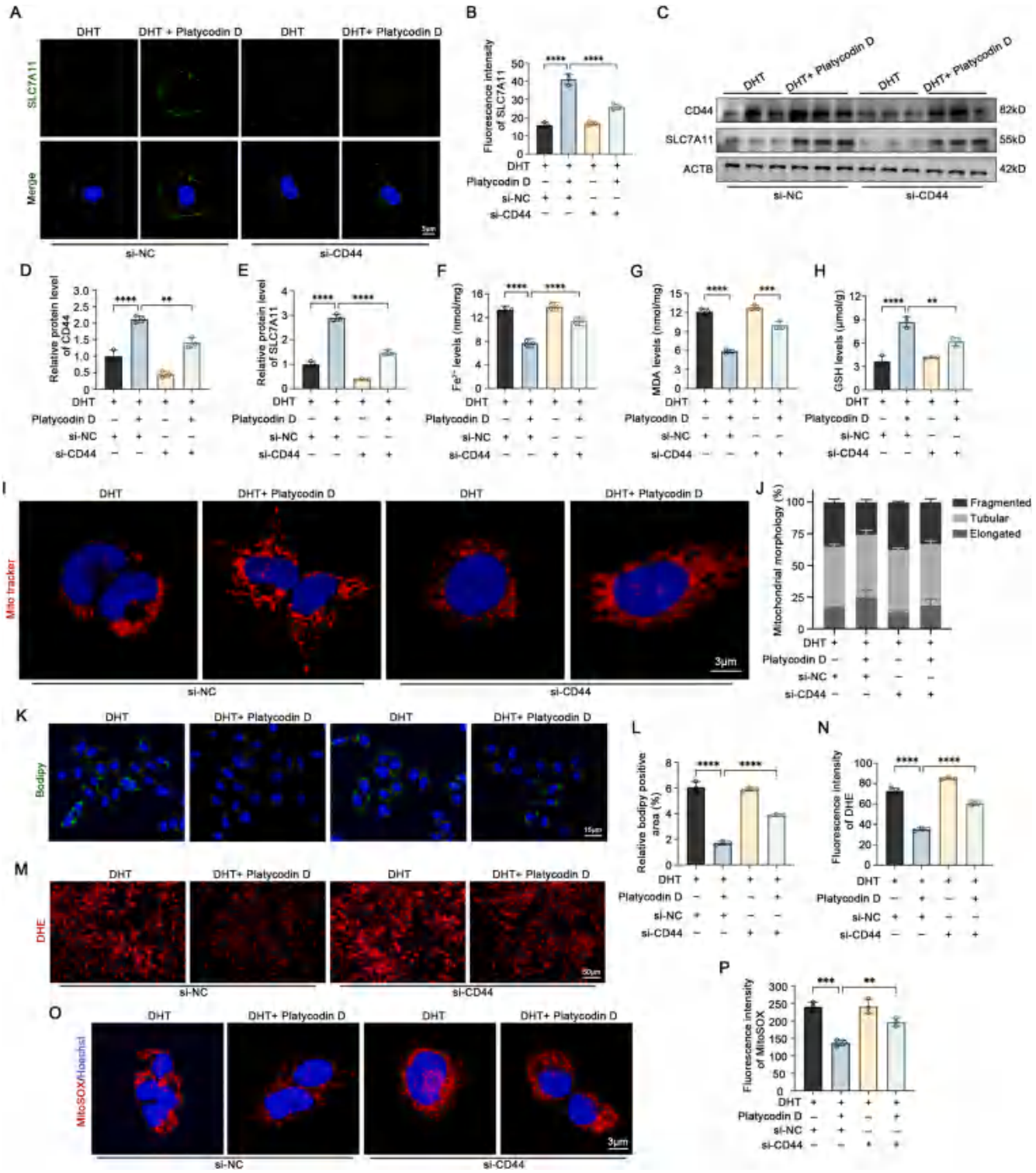

Fig. 6. Platycodin D ameliorates ferroptosis in KGN cells by targeting CD44

A, B. The levels of SLC7A11 in KGN cells were detected by immunofluorescence staining (n = 3). C-E. Western blot and densitometric analysis for the expression of CD44, and SLC7A11 in KGN cells (n = 3). F-H. MDA, Fe^{2+} and GSH levels in KGN cells (n = 3). I, J. Representative confocal microscopy image of MitoTracker Red staining in KGN cells (n = 3). K, L. Lipid accumulation in KGN cells was detected by BODIPY probe (n = 3). M, N. ROS levels in KGN cells were detected using DHE probe (n = 3). O, P. ROS levels of mitochondria in KGN cells were detected using MitoSOX probe (n = 3). one-way ANOVA. **p < 0.01; ***p < 0.001; ****p < 0.0001.

(Fig. 6K and L). DHE staining revealed that CD44 silencing significantly attenuated ROS removal by platycodin D (Fig. 6M and N). Furthermore, MitoSOX staining revealed that the effect of mitochondrial ROS scavenging by platycodin D was partially reversed by CD44 siRNA (Fig. 6O and P).

To further investigate whether platycodin D ameliorates ferroptosis in KGN cells via the activation of CD44/SLC7A11, we transfected KGN cells with SLC7A11 siRNA which had the best knockdown efficiency

(Supplementary Fig. 6 D-F). Immunofluorescence and western blotting assays revealed that the increase of SLC7A11 treated with platycodin D was reversed significantly by SLC7A11 siRNA (Supplementary Fig. 7A-C, E). However, the change in CD44 expression was not significantly affected (Supplementary Figs. 7C and D). Based on the changes in CD44 and SLC7A11 expression in KGN cells following CD44 knockdown, we hypothesize that platycodin D exerts its effects by activating SLC7A11 via CD44. We administered identical treatment following the knockdown of SLC7A11 and evaluated the levels of MDA, Fe^{2+}, GSH, mitochondrial fission, ROS, and lipids in KGN. The results revealed that SLC7A11 knockdown inhibited the effects of platycodin D in ameliorating Fe^{2+} accumulation, mitochondrial fragmentation, ROS production in the cytoplasm and mitochondria, lipid accumulation, and lipid peroxidation in KGN cells (Supplementary Figs. 7I–P).

Consequently, by knocking down SLC7A11 and CD44 for cellular functionality experiments, we found that platycodin D alleviates DHT-induced ferroptosis in KGN cells via the activation of CD44/SLC7A11.

3.8. Platycodin D alleviates ferroptosis in PCOS rats by targeting CD44/SLC7A11

To elucidate the potential mechanism by which Platycodin D alleviates symptoms in PCOS rats, we locally injected knockdown lentiviruses of CD44 and SLC7A11 into the ovaries of rats, followed by DHT treatment and tangerine saponin D treatment, respectively (Fig. 7A).

The results showed that the knockdown of CD44 and SLC7A11 in the ovary inhibited the effects of platycodin D, including reductions in body weight, amelioration of androgen elevation, and restoration of the estrous cycle in PCOS rats (Fig. 7B–E). Additionally, the beneficial effects of platycodin D on follicular development in rats with PCOS were reversed by silencing CD44 or SLC7A11 (Fig. 7F–I).

Immunohistochemical analysis showed that 4HNE levels were significantly lower in the ovaries of rats with PCOS treated with platycodin D than in the PCOS group. Conversely, 4HNE levels were significantly higher in the ovaries of rats with PCOS and CD44 or SCL7A11 knockdown in the ovaries than in rats treated with platycodin D (Fig. 8A and B). Additionally, the local knockdown of CD44 or SLC7A11 in ovaries inhibited the ability of platycodin D to clear ovarian ROS in rats with PCOS (Fig. 8C and D).

Transmission electron microscopy revealed that the improvements in damage, including the swelling of mitochondria and disorganization of cristae, by platycodin D were not observed in rats injected with CD44 shRNA and SLC7A11 shRNA lentivirus (Fig. 8E and F). Additionally, the ability of platycodin D to eliminate MDA and Fe^{2+} and restore GSH from

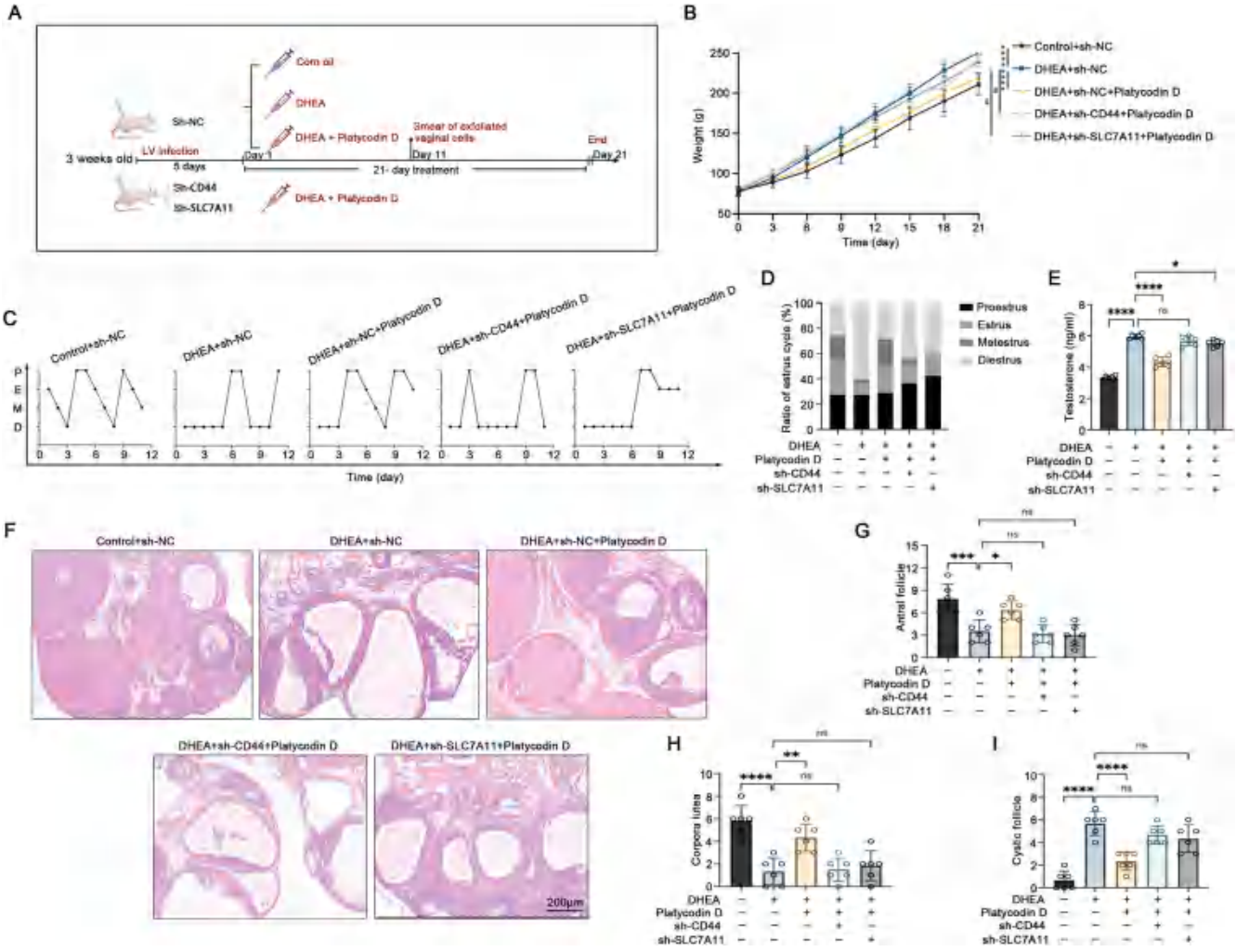

Fig. 7. Platycodin D Reduce PCOS damage in rats by targeting CD44/SLC7A11
A. Exploration of the effect of CD44 and SLC7A11 knockdown on the treatment of platycodin D in PCOS rats. B. The changes of body weight of rats in each group (n = 6). C, D. Estrous cycle of each group of rats (n = 6). E. Serum testosterone levels in rats (n = 6). F. Morphological observation of ovary in rats (n = 6). G-I. The number of antral follicles, corpora lutea and cystic follicles in each group was statistically analyzed. (n = 6). one-way ANOVA. *p < 0.05; **p < 0.01; ***p < 0.001; ****p < 0.0001; ns, not significant.

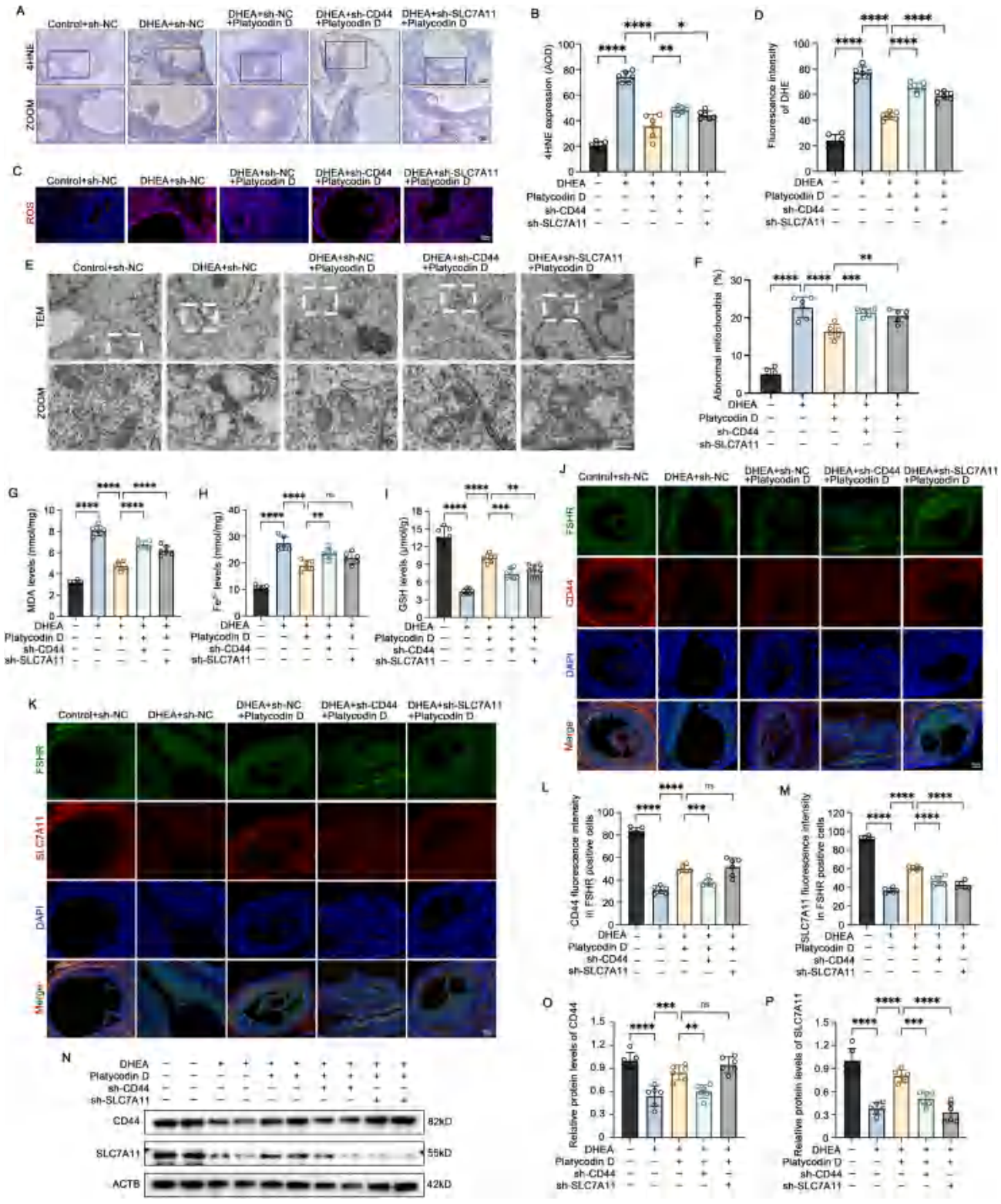

Fig. 8. Platycodin D ameliorates ferroptosis in PCOS rats by targeting CD44/SLC7A11

A, B. Immunohistochemical analysis of 4HNE expression in the ovaries of rats (n = 6). C, D. ROS levels fo ovaries in rats were detected using DHE probe (n = 6). E, F. Mitochondria of GCs in rat ovarian tissue were observed by TEM (n = 6). G-I. MDA, Fe^{2+} and GSH levels of ovaries in each group of rats (n = 6). J-M. The levels of CD44 and SLC7A11 in rat ovarian GCs were detected by immunofluorescence staining (n = 6). N-P. Western blot and densitometric analysis for the expression of CD44, and SLC7A11 in the ovaries of each rat (n = 3). one-way ANOVA. *p < 0.05; **p < 0.01; ***p < 0.001; ****p < 0.0001; ns, not significant.

the ovaries of rats with PCOS was impeded by the knockdown of CD44 and SLC7A11 (Fig. 8G–I). Immunofluorescence staining and western blotting assays confirmed that CD44 and SLC7A11 levels were significantly reduced in the ovarian GCs of rats with PCOS. Furthermore, platycodin D treatment led to a partial restoration of CD44 and SLC7A11 levels. Nevertheless, the restoration of CD44 and SLC7A11 was significantly inhibited in platycodin D-treated rats with CD44 lentiviral knockdown. Additionally, the recovery of SLC7A11 was inhibited in the rats with SLC7A11 lentiviral knockdown in the platycodin D treatment group. However, the recovery of CD44 was not significantly inhibited (Fig. 8J–M). Western blotting results were consistent with immunofluorescence staining results (Fig. 8N–P). These results, along with those of the previous experiments, suggest that platycodin D ameliorates ferroptosis in PCOS rats by activating CD44/SLC7A11.

4. Discussion

PCOS is a reproductive endocrine disease affecting women of reproductive age. It has garnered considerable attention in recent years. In this study, to the best of our knowledge, we demonstrate for the first time that CD44 down-regulation results in ferroptosis in GCs in PCOS. We screened the platycodin D, which activates CD44, using molecular docking, kinetic simulation, and functional experiments. Our results indicate that platycodin D can alleviate ferroptosis and mitigate associated injuries in PCOS by activating the CD44/SLC7A11 pathway, which was shown in both *in vivo* and *in vitro* experiments. These findings provide novel insights into the mechanisms underlying ferroptosis in PCOS.

Ferroptosis is characterized by an imbalance in cellular redox homeostasis, associated with a disruption in iron metabolism and resulting in lipid peroxidation. Under normal conditions, cells uptake Fe^{2+} via the interaction of transferrin (TF) and transferrin receptor 1 (TFR1), leading to its entry into the nuclear endosome. Here, Fe^{3+} is converted back to Fe^{2+} by prostate six-transmembrane epithelial antigen 3 (STEAP3), forming a labile iron pool (LIP). A portion of this Fe^{2+} in the LIP is used in mitochondrial processes, whereas the remainder is stored in ferritin. However, in pathological scenarios, disruptions in iron metabolism lead to intracellular iron overload, triggering the Fenton reaction and the generation of hydroxyl radicals, resulting in cellular lipid peroxidation, oxidative DNA damage, and ultimately, cell death [30]. Since its inception, ferroptosis has shown promise in tumor suppression and immune surveillance due to its close association with cellular metabolic processes such as redox, glucose, lipid, and amino acid metabolism [5]. Recent advancements in research on ischemic organ damage, metabolic disorders, and degenerative diseases have highlighted the potential of modulating ferroptosis induction or inhibition as a novel therapeutic approach to mitigate pathological damage and promote healing [31]. PCOS is a reproductive endocrine disorder of unknown etiology that is often characterized by reproductive dysfunction, insulin resistance, abnormalities in glucose and lipid metabolism, and obesity, among other metabolic abnormalities. Given the increasing attention to ferroptosis in PCOS research, it has been observed that patients with PCOS exhibit increased iron levels and increased ROS production in GCs, suggesting a potential association between PCOS and ferroptosis [32,33]. Studies have identified changes in ferroptosis regulatory molecules, including GPX4 and SLC7A11, in the GCs of patients with PCOS and rat models. Additionally, increased 4HNE, the major product of lipid peroxidation, was observed in the ovaries of rats with PCOS. These findings imply a potential involvement of ferroptosis in the pathogenesis of PCOS.

GSH is a widely recognized antioxidant that is synthesised continuously from glutamate, cysteine, and glycine under the catalysis of glutamate-cysteine ligase. Given the restricted concentration of cysteine under physiological conditions, cysteine plays a pivotal role as a rate-limiting precursor in the synthesis of GSH [34]. The system X_c^- is a heterodimeric protein complex, comprising SLC7A11/xCT and SLC3A2. SLC7A11 plays a central role in the system X_c^- as a sodium-independent reverse transporter that facilitates the transcellular transport of glutamate and cystine. Then, cystine is converted into cysteine within the cell under conditions of intracellular reduction, providing the essential raw materials for GSH biosynthesis [35]. Under physiological conditions, SLC7A11 functions as a classical regulator of ferroptosis, inhibiting this form of cell death by facilitating redox reactions. Recent investigations on ferroptosis-related regulatory pathways and defense mechanisms have revealed a growing number of molecules with potential as targets for ferroptosis regulation. CD44, a family of non-kinase transmembrane glycoproteins initially identified in embryonic stem cells, has garnered significant attention. The interaction of CD44 with its ligand hyaluronan activates multiple signal transduction pathways, promoting cell proliferation, migration, and invasion, making it a promising candidate for tumor progression and targeted therapy [13]. Notably, emerging research indicates that CD44 not only regulates cell stemness and migratory properties but also inhibits the ferroptosis of tumor cells and promotes cancer progression by improving the stability of SLC7A11 [18]. In this study, we observed downregulation of SLC7A11 expression in the GCs of patients with PCOS and ovaries of PCOS rats, resulting in ferroptosis in GCs. Furthermore, the activation of SLC7A11 by targeting CD44 has been demonstrated to reduce ferroptosis in GCs in both *in vivo* and *in vitro* experiments. Our study provides insights into the crucial role of platycodin D in inhibiting ferroptosis in GCs by regulating the activity of the system X_c^- via CD44.

The diverse structural and chemical properties found in natural plants and their derived compounds have led to their use as a significant resource for drug discovery. The integration of bioinformatics-based and virtual screening strategies has facilitated the identification of natural plant drugs as promising candidates for the discovery of potential therapeutic agents across various diseases [36,37]. Initial screening of bioinformatics data can identify key regulatory molecules involved in disease development and progression. Then, molecular docking and kinetic simulation can find matching compounds from databases, which can help identify drug targets for diseases [38]. *Platycodon grandiflorum* is a food with a long history in the East. The rhizome and leaves of *Platycodon grandiflorum* possess high practical value. Additionally, the medicinal value of *Platycodon grandiflorum* is widely recognized and used in numerous herbal formulas [39]. Platycodin D, one of the principal active ingredients derived from *Platycodon grandiflorum*, is an oleanane-type triterpenoid saponin known to possess antiviral, antitumor, and anti-inflammatory properties [40,41]. Moreover, Platycodin D has shown promise in improving metabolic diseases such as coronary heart disease attributed to its anti-obesity and hypoglycemic effects [42]. Recent studies have revealed its potential to reduce high glucose-induced ferroptosis in HK2 cells [23]. In this study, we used bioinformatics analysis and validation in clinical specimens and animal models to identify CD44 as a pivotal regulator of ferroptosis in GCs in PCOS development. Through a search for natural phytopharmaceuticals from databases known to attenuate ferroptosis, we identified several small-molecule compounds best matching CD44 through molecular docking simulations. Comparing the activation of CD44 by candidate drugs in GCs via western blotting, platycodin D was identified as an effective drug for targeting CD44 to alleviate ferroptosis in GCs in PCOS as supported by molecular dynamics simulation and CETSA. Subsequently, *in vivo* studies revealed that platycodin D mitigates the pathological phenotype of PCOS by improving ferroptosis in GCs. Moreover, *in vivo* and *in vitro* experiments have demonstrated that platycodin D exerts its protective effects primarily through the activation of the CD44/SLC7A11 axis, which in turn activates the GSH antioxidant system, reduces lipid peroxidation, and ultimately protects GCs from ferroptosis.

Despite the significant findings in our study, several limitations should be addressed. While we observed that platycodin D reduced intracellular iron overload, the precise mechanism by which it regulates iron ions is not yet elucidated. Furthermore, recent studies on ferroptosis

have highlighted phospholipid hydroperoxides (PLOOH) as direct executors of ferroptosis, with GPX4 playing a crucial role in neutralizing PLOOH triggers cell death by causing irreversible damage to the plasma membrane [43]. However, GPX4, a major PLOOH-neutralizing enzyme, prevents PLOOH damage to the plasma membrane by catalyzing the conversion of GSH to GSSG, mediating the reduction of PLOOH to the corresponding alcohol, PL-OH [44]. In the present study, we found a decrease in ferroptosis regulatory proteins, such as GPX4, in the GCs of patients with PCOS and the ovarian tissues of rats with PCOS. Platycodin D can restore GSH synthesis by activating the X_c^- system, thereby protecting the cells against oxidative stress damage. Nevertheless, we did not observe a restorative effect of platycodin D on GPX4. Previous studies have shown that the ferroptosis suppressor protein 1 (FSP1)/ubiquinone system prevents ferroptosis triggered by GPX4 knockdown [45]. We postulated that platycodin D may attenuate lipid oxidative damage in cells via a GPX4-independent pathway, in addition to activating the X_c^- system. Furthermore, the present study examined the impact of CD44 activation by platycodin D on the X_c^- system. Recent studies have indicated that variant isoforms of CD44 are also involved in the activation of PI3K/AKT, ERK1/2 MAP, and other kinase pathways. These signalling pathways have been found to be closely related to the regulation of ferroptosis [46]. Therefore, we hypothesize that platycodin D might alleviate ferroptosis in GCs by affecting CD44 isoforms and activating downstream signalling pathways. However, these possibilities need to be confirmed by further studies.

To conclude, to the best of our knowledge, this is the first study to investigate the potential ameliorative effect of platycodin D on ferroptosis of GCs in PCOS. Our findings indicate that platycodin D attenuates ferroptosis in GCs by targeting CD44 to activate the X_c^- system, which alleviases the pathological damage associated with PCOS. Our findings provide novel insights into ferroptosis in PCOS.

Data availability

The datasets used during the current study are available from the corresponding author on reasonable request.

Ethics approval

The experiments conducted in this study were ethically approved by the Ethics Committee of Wuhan University People's Hospital (Wuhan, China, WDRY2019-K077). All animal experiments were designed in accordance with the Guidelines for the Use of Laboratory Animal Care (No. 20210307) and strictly performed according to the Guide for the Care and Use of Laboratory Animals published by the US National Institutes of Health.

Consent for publication

Not applicable.

CRediT authorship contribution statement

Rui Ji: Writing – original draft, Methodology, Data curation. **Shujun Wang:** Visualization, Formal analysis. **Xin Chen:** Writing – review & editing. **Zhe Yang:** Methodology, Data curation. **Zhimo Zhang:** Data curation. **Shenglan Bao:** Software. **Zhuoni Xiao:** Supervision, Investigation. **Yan Zhang:** Validation, Investigation. **Tailang Yin:** Project administration, Funding acquisition. **Jing Yang:** Resources, Project administration.

Declaration of interest statement

We declare that we have no financial and personal relationships with other people or organizations that can inappropriately influence our work, there is no professional or other personal interest of any nature or kind in any product, service and/or company that could be construed as influencing the position presented in, or the review of, the manuscript entitled "**Platycodin D ameliorates polycystic ovary syndrome-induced ovarian damage by** upregulating **CD44 to attenuate ferroptosis"**.

Acknowledgements

This work was financially supported by the National Natural Science Foundation of China (Grant No. 81971356,82271672, 81771662, 81771618), the National Key Research and Development Program of China (No. 2016YFC1000600, 2018YFC1002804), the Key Research & Developmental Program of of Hubei Province (2022BCA042), the Fundamental Research Funds for the Central Universities (2042022kf1210), and the Interdisciplinary Innovative Talents Foundation from Renmin Hospital of Wuhan University (JCRCWL-2022-001). Figures created with Biorender. Com.

Appendix A. Supplementary data

Supplementary data to this article can be found online at https://doi.org/10.1016/j.freeradbiomed.2024.09.033.

References

[1] M. Dapas, A. Dunaif, Deconstructing a syndrome: genomic insights into PCOS causal mechanisms and classification, Endocr. Rev. 43 (6) (2022) 927–965.
[2] N. Gleicher, S. Darmon, P. Patrizio, D.H. Barad, Reconsidering the polycystic ovary syndrome (PCOS), Biomedicines 10 (7) (2022).
[3] A. Joshi, PCOS stratification for precision diagnostics and treatment, Front. Cell Dev. Biol. 12 (2024) 1358755.
[4] Y. Jiang, J. Yang, K. Du, K. Luo, X. Yuan, F. Hua, 1,25-Dihydroxyvitamin D3 alleviates hyperandrogen-induced ferroptosis in KGN cells, Hormones (Basel) 22 (2) (2023) 273–280.
[5] X. Jiang, B.R. Stockwell, M. Conrad, Ferroptosis: mechanisms, biology and role in disease, Nat. Rev. Mol. Cell Biol. 22 (4) (2021) 266–282.
[6] L. Xie, B. Fang, C. Zhang, The role of ferroptosis in metabolic diseases, Biochim. Biophys. Acta Mol. Cell Res. 1870 (6) (2023) 119480.
[7] F. Wang, Y. Liu, F. Ni, J. Jin, Y. Wu, Y. Huang, X. Ye, X. Shen, Y. Ying, J. Chen, R. Chen, Y. Zhang, X. Sun, S. Wang, X. Xu, C. Chen, J. Guo, D. Zhang, BNC1 deficiency-triggered ferroptosis through the NF2-YAP pathway induces primary ovarian insufficiency, Nat. Commun. 13 (1) (2022) 5871.
[8] J. Huang, H. Fan, C. Li, K. Yang, C. Xiong, S. Xiong, S. Feng, S. Chen, B. Wang, Y. Su, B. Xu, H. Yang, N. Wang, J. Zhu, Dysregulation of ferroptosis-related genes in granulosa cells associates with impaired oocyte quality in polycystic ovary syndrome, Front. Endocrinol. 15 (2024) 1346842.
[9] Y. Zhang, M. Hu, W. Jia, G. Liu, J. Zhang, B. Wang, J. Li, P. Cui, X. Li, S. Lager, A. N. Sferruzzi-Perri, Y. Han, S. Liu, X. Wu, M. Brannstrom, L.R. Shao, H. Billig, Hyperandrogenism and insulin resistance modulate gravid uterine and placental ferroptosis in PCOS-like rats, J. Endocrinol. 246 (3) (2020) 247–263.
[10] W. Tan, F. Dai, D. Yang, Z. Deng, R. Gu, X. Zhao, Y. Cheng, MiR-93-5p promotes granulosa cell apoptosis and ferroptosis by the NF-kB signaling pathway in polycystic ovary syndrome, Front. Immunol. 13 (2022) 967151.
[11] Q. Peng, X. Chen, X. Liang, J. Ouyang, Q. Wang, S. Ren, H. Xie, C. Wang, Y. Sun, X. Wu, H. Liu, C. Hei, M. Sun, Q. Chang, X. Liu, G. Li, R. He, Metformin improves polycystic ovary syndrome in mice by inhibiting ovarian ferroptosis, Front. Endocrinol. 14 (2023) 1070264.
[12] Y. Xu, Z. Bai, T. Lan, C. Fu, P. Cheng, CD44 and its implication in neoplastic diseases, MedComm 5 (6) (2020) e554, 2024.
[13] X. Weng, S. Maxwell-Warburton, A. Hasib, L. Ma, L. Kang, The membrane receptor CD44: novel insights into metabolism, Trends Endocrinol Metab 33 (5) (2022) 318–332.
[14] Q. Guo, C. Yang, F. Gao, The state of CD44 activation in cancer progression and therapeutic targeting, FEBS J. 289 (24) (2022) 7970–7986.
[15] B. Han, S. Zhou, Y. Zhang, S. Chen, W. Xi, C. Liu, X. Zhou, M. Yuan, X. Yu, L. Li, Y. Wang, H. Ren, J. Xie, B. Li, M. Ju, Y. Zhou, Z. Liu, Z. Xiong, L. Shen, Y. Zhang, Y. Bai, J. Chen, W. Jiang, H. Yao, Integrating spatial and single-cell transcriptomics to characterize the molecular and cellular architecture of the ischemic mouse brain, Sci. Transl. Med. 16 (733) (2024) eadg1323.
[16] X. Weng, H. Jiang, D.J. Walker, H. Zhou, D. Lin, J. Wang, L. Kang, Deletion of CD44 promotes adipogenesis by regulating PPARgamma and cell cycle-related pathways, J. Endocrinol. 262 (1) (2024).
[17] F. Lin, W. Chen, J. Zhou, J. Zhu, Q. Yao, B. Feng, X. Feng, X. Shi, Q. Pan, J. Yu, L. Li, H. Cao, Mesenchymal stem cells protect against ferroptosis via exosome-mediated stabilization of SLC7A11 in acute liver injury, Cell Death Dis. 13 (3) (2022) 271.
[18] T. Liu, L. Jiang, O. Tavana, W. Gu, The deubiquitylase OTUB1 mediates ferroptosis via stabilization of SLC7A11, Cancer Res. 79 (8) (2019) 1913–1924.

[19] W. Deng, J. Ai, W. Zhang, Z. Zhou, M. Li, L. Yan, L. Zhang, Z. Huang, Z. Wu, J. Ai, H. Jiang, Arginine methylation of HSPA8 by PRMT9 inhibits ferroptosis to accelerate hepatitis B virus-associated hepatocellular carcinoma progression, J. Transl. Med. 21 (1) (2023) 625.
[20] V. Stepanic, M. Kucerova-Chlupacova, Review and chemoinformatic analysis of ferroptosis modulators with a focus on natural plant products, Molecules 28 (2) (2023).
[21] K. Yang, L. Zeng, J. Zeng, Y. Deng, S. Wang, H. Xu, Q. He, M. Yuan, Y. Luo, A. Ge, J. Ge, Research progress in the molecular mechanism of ferroptosis in Parkinson's disease and regulation by natural plant products, Ageing Res. Rev. 91 (2023) 102063.
[22] Y.W. Lu, L.Y. Xie, M.H. Qi, S. Ren, Y.Q. Wang, J.N. Hu, Z. Wang, S. Tang, J. T. Zhang, W. Li, Platycodin D ameliorates cognitive impairment in type 2 diabetes mellitus mice via regulating PI3K/Akt/GSK3beta signaling pathway, J. Agric. Food Chem. 72 (22) (2024) 12516–12528.
[23] J. Huang, G. Chen, J. Wang, S. Liu, J. Su, Platycodin D regulates high glucose-induced ferroptosis of HK-2 cells through glutathione peroxidase 4 (GPX4), Bioengineered 13 (3) (2022) 6627–6637.
[24] R. Ji, Z. Zhang, Z. Yang, X. Chen, T. Yin, J. Yang, BOP1 contributes to the activation of autophagy in polycystic ovary syndrome via nucleolar stress response, Cell. Mol. Life Sci. 81 (1) (2024) 101.
[25] R. Ji, F. Jia, X. Chen, Y. Gao, J. Yang, Carnosol inhibits KGN cells oxidative stress and apoptosis and attenuates polycystic ovary syndrome phenotypes in mice through Keap1-mediated Nrf2/HO-1 activation, Phytother Res. 37 (4) (2023) 1405–1421.
[26] H.B. Park, S. Hwang, K.H. Baek, USP7 regulates the ERK1/2 signaling pathway through deubiquitinating Raf-1 in lung adenocarcinoma, Cell Death Dis. 13 (8) (2022) 698.
[27] X. Li, Y. Lin, X. Cheng, G. Yao, J. Yao, S. Hu, Q. Zhu, Y. Wang, Y. Ding, Y. Lu, J. Qi, H. Zhao, X. Bian, Y. Du, K. Sun, H. Vankelecom, Y. Sun, Ovarian ferroptosis induced by androgen is involved in pathogenesis of PCOS, Hum Reprod Open 2024 (2) (2024) hoae013.
[28] Z. Guo, S. Wang, H. Hao, X. Deng, J. Fu, Y. Guo, Y. Yuan, Y. Jiao, S. Han, Targeting ferroptosis in cancer by natural products: an updated review, Am. J. Chin. Med. 51 (3) (2023) 547–574.
[29] Z. Bian, X. Sun, L. Liu, Y. Qin, Q. Zhang, H. Liu, L. Mao, S. Sun, Sodium butyrate induces CRC cell ferroptosis via the CD44/slc7a11 pathway and exhibits a synergistic therapeutic effect with erastin, Cancers 15 (2) (2023).
[30] D. Tang, X. Chen, R. Kang, G. Kroemer, Ferroptosis: molecular mechanisms and health implications, Cell Res. 31 (2) (2021) 107–125.
[31] X. Chen, R. Kang, G. Kroemer, D. Tang, Ferroptosis in infection, inflammation, and immunity, J. Exp. Med. 218 (6) (2021).
[32] D.F. Al-Akabi, H.A. Hafth, Physiological effect of iron status on patients with polycystic ovary syndrome in Basrah city, J. Med. Biochem. 42 (3) (2023) 530–535.
[33] C. Banuls, S. Rovira-Llopis, A. Martinez de Maranon, S. Veses, A. Jover, M. Gomez, M. Rocha, A. Hernandez-Mijares, V.M. Victor, Metabolic syndrome enhances endoplasmic reticulum, oxidative stress and leukocyte-endothelium interactions in PCOS, Metabolism 71 (2017) 153–162.
[34] I. Costa, D.J. Barbosa, S. Benfeito, V. Silva, D. Chavarria, F. Borges, F. Remiao, R. Silva, Molecular mechanisms of ferroptosis and their involvement in brain diseases, Pharmacol. Ther. 244 (2023) 108373.
[35] R.J. Wen, X. Dong, H.W. Zhuang, F.X. Pang, S.C. Ding, N. Li, Y.X. Mai, S.T. Zhou, J. Y. Wang, J.F. Zhang, Baicalin induces ferroptosis in osteosarcomas through a novel Nrf2/xCT/GPX4 regulatory axis, Phytomedicine 116 (2023) 154881.
[36] B. Shaker, S. Ahmad, J. Lee, C. Jung, D. Na, In silico methods and tools for drug discovery, Comput. Biol. Med. 137 (2021) 104851.
[37] A. Bruno, G. Costantino, L. Sartori, M. Radi, The in silico drug discovery toolbox: applications in lead discovery and optimization, Curr. Med. Chem. 26 (21) (2019) 3838–3873.
[38] L. Zhang, J. Song, L. Kong, T. Yuan, W. Li, W. Zhang, B. Hou, Y. Lu, G. Du, The strategies and techniques of drug discovery from natural products, Pharmacol. Ther. 216 (2020) 107686.
[39] L. Feng, Y. Shi, J. Zou, X. Zhang, B. Zhai, D. Guo, J. Sun, M. Wang, F. Luan, Recent advances in Platycodon grandiflorum polysaccharides: preparation techniques, structural features, and bioactivities, Int. J. Biol. Macromol. 259 (Pt 1) (2024) 129047.
[40] C. Bailly, The implication of the PD-1/PD-L1 checkpoint in chronic periodontitis suggests novel therapeutic opportunities with natural products, Jpn Dent Sci Rev 56 (1) (2020) 90–96.
[41] R. Guo, Q. Meng, B. Wang, F. Li, Anti-inflammatory effects of Platycodin D on dextran sulfate sodium (DSS) induced colitis and E. coli Lipopolysaccharide (LPS) induced inflammation, Int Immunopharmacol 94 (2021) 107474.
[42] Y.J. Choi, S.J. Lee, H.I. Kim, H.J. Lee, S.J. Kang, T.Y. Kim, C. Cheon, S.G. Ko, Platycodin D enhances LDLR expression and LDL uptake via down-regulation of IDOL mRNA in hepatic cells, Sci. Rep. 10 (1) (2020) 19834.
[43] M. Conrad, D.A. Pratt, The chemical basis of ferroptosis, Nat. Chem. Biol. 15 (12) (2019) 1137–1147.
[44] Y. Wang, L. Zheng, W. Shang, Z. Yang, T. Li, F. Liu, W. Shao, L. Lv, L. Chai, L. Qu, Q. Xu, J. Du, X. Liang, J. Zeng, J. Jia, Wnt/beta-catenin signaling confers ferroptosis resistance by targeting GPX4 in gastric cancer, Cell Death Differ. 29 (11) (2022) 2190–2202.
[45] S. Doll, F.P. Freitas, R. Shah, M. Aldrovandi, M.C. da Silva, I. Ingold, A. Goya Grocin, T.N. Xavier da Silva, E. Panzilius, C.H. Scheel, A. Mourao, K. Buday, M. Sato, J. Wanninger, T. Vignane, V. Mohana, M. Rehberg, A. Flatley, A. Schepers, A. Kurz, D. White, M. Sauer, M. Sattler, E.W. Tate, W. Schmitz, A. Schulze, V. O'Donnell, B. Proneth, G.M. Popowicz, D.A. Pratt, J.P.F. Angeli, M. Conrad, FSP1 is a glutathione-independent ferroptosis suppressor, Nature 575 (7784) (2019) 693–698.
[46] J. Weng, Q. Liu, C. Li, Y. Feng, Q. Chang, M. Xie, X. Wang, M. Li, H. Zhang, R. Mao, N. Zhang, X. Yang, K.F. Chung, I.M. Adcock, Y. Huang, F. Li, TRPA1-PI3K/Akt-OPA1-ferroptosis axis in ozone-induced bronchial epithelial cell and lung injury, Sci. Total Environ. 918 (2024) 170668.